

Computational Validation of the Oloid as a Local Optimum in the Developable Roller Family

Contact Distribution Score: A Formal Metric for Evaluating
Geometric Primitives as Engineering Substrate

Vincent Wesley Couey

Substrate Geometry Research Program

vinnycouey@gmail.com

<https://github.com/gyapaganda-a11y/substrate-geometry>

May 5, 2026 – Preprint (not peer-reviewed)

Abstract

Many engineering failures (thermal hotspot concentration, Hertz contact fatigue localization, boundary-layer loss, mixing dead zones) are *geometric failure modes*: changing the material delays the failure; changing the geometry eliminates it. Despite this, no formal metric exists for evaluating how uniformly a convex body distributes surface contact during rolling, a property with direct implications for bearing wear, seal longevity, and fluid mixing efficiency.

We introduce the **Contact Distribution Score (CDS)**, a scalar metric defined as the area-weighted variance of the contact time distribution over a rolling surface, and its stress-domain counterpart the **Stress Distribution Score (SDS)**, defined as the area-weighted variance of accumulated Hertz contact pressure. $CDS \rightarrow 0$ indicates perfectly uniform contact; $SDS \rightarrow 0$ indicates perfectly uniform stress.

We implement a three-layer oracle architecture: an approximate oracle for parametric search, a rigid-body oracle using Euler-equation dynamics with quaternion integration for validation, and a Hertz contact pressure oracle that couples discrete surface curvature analysis with analytical Hertz theory to evaluate stress distribution. A parametric search over 45 members of the developable roller family (closed convex surfaces formed by the convex hull of two circles) identifies the oloid (Schatz, 1929) at $CDS = 8.2 \times 10^{-7}$ under rigid-body dynamics, with the conventional cylinder baseline at 4.75×10^{-5} , a $58\times$ discrimination. Independent curvature-driven stress analysis confirms that the contact time invariant transfers to stress distribution: under perfectly uniform contact, the oloid's geometry-only SDS is 4.8×10^{-8} , confirming that the oloid's surface curvature introduces minimal additional stress non-uniformity beyond the contact distribution itself. We extend this analysis to fatigue (FDS), thermal (TDS), and wear (WDS) distribution scores, revealing that the oloid's $58\times$ CDS advantage transfers consistently across all physical transforms, with discrimination ratios in the $46\text{--}68\times$ range across linear and multiplicative metrics. The nonlinear fatigue metric diverges due to Basquin S-N amplification but still shows oloid superiority over all tested alternatives.

This work establishes the formal vocabulary and computational infrastructure for *substrate geometry*: the study of geometric forms as engineering substrates classified by their operational invariants.

Keywords: contact distribution, stress distribution, Hertz contact, geometric primitives, oloid, developable surfaces, rigid-body rolling, invariant-based design, substrate geometry

arXiv categories: math-ph, cs.CG, math.MG

Contents

| | | |
|----------|---|-----------|
| 1 | Introduction | 2 |
| 1.1 | Contributions | 3 |
| 2 | Definitions | 3 |
| 3 | The Contact Distribution Oracle | 5 |
| 3.1 | Architecture | 5 |
| 3.2 | Approximate Oracle | 5 |
| 3.3 | Rigid-Body Oracle | 5 |
| 3.3.1 | Parameters | 6 |
| 4 | The Developable Roller Family | 6 |
| 4.1 | Search Grid | 7 |
| 5 | Results | 7 |
| 5.1 | Approximate Oracle Search | 7 |
| 5.2 | Rigid-Body Oracle Validation | 7 |
| 5.3 | Parameter Sensitivity | 8 |
| 5.4 | Two-Layer Architecture Validation | 8 |
| 5.5 | Hertz Contact Pressure Validation | 9 |
| 5.6 | Fatigue, Thermal, and Wear Distribution | 9 |
| 6 | Discussion | 10 |
| 6.1 | The Oloid as Local Optimum | 10 |
| 6.2 | Substrate Geometry as a Design Paradigm | 11 |
| 6.3 | Limitations | 11 |
| 6.4 | Future Work | 12 |
| 7 | Conclusion | 12 |
| A | Reproducibility | 13 |
| B | Full Search Results | 13 |

1 Introduction

Engineering systems fail for many reasons, but a significant class of failures can be traced to a root cause that is neither the material nor the power source but the *geometry* of the component. Thermal hotspot concentration on flat-plate electrodes, Hertz contact fatigue at the fixed loci of cylindrical bearings, Hartmann boundary-layer losses in rectangular MHD ducts, and mixing dead zones in conventional stirred tanks are all instances of what we term *geometric failure modes*.

Definition 1 (Geometric Failure Mode). *A class of engineering failure whose root cause is the geometry of the component rather than the material or power source. The defining characteristic: changing the material delays the failure; changing the geometry eliminates it.*

The conventional engineering response to geometric failure modes is to upgrade the material: higher-temperature alloys, harder bearing steels, more corrosion-resistant coatings. This approach treats the symptom. An alternative, demonstrated empirically by Paul Schatz’s oloid [1] and the gyroid heat exchanger [2], is to select a geometry whose mathematical invariants preclude the failure mode at source.

The oloid (the convex hull of two perpendicular circles of equal radius, each passing through the other’s center) was discovered by Schatz in 1929 through geometric intuition and physical experimentation.¹ Its defining property is that every point on its surface makes contact with the ground plane during one complete roll, distributing contact uniformly across its entire surface. This property directly eliminates the Hertz fatigue localization that limits conventional cylindrical bearings and has been exploited commercially in water aeration (Oloid AG) and laboratory mixing (Turbula shaker-mixer).

Despite the oloid’s demonstrated utility, no formal metric has existed for *quantifying* how uniformly a convex body distributes contact. This paper introduces such a metric, builds the computational infrastructure to evaluate it, and uses it to confirm that the oloid is a local optimum within its geometric search family.

1.1 Contributions

1. We define the **Contact Distribution Score (CDS)**, a scalar metric for contact uniformity during rolling, expressed as a computable predicate suitable for optimization.
2. We implement a **three-component oracle architecture**: a two-layer CDS oracle (an approximate layer for fast parametric search and a rigid-body layer using Euler-equation dynamics for validation), plus a separate Hertz contact pressure oracle for independent SDS validation.
3. We conduct a **parametric search** over 45 members of the developable roller family, varying circle-plane angle, offset, and radius ratio.
4. We **computationally confirm** that the oloid (Schatz, 1929) occupies a local CDS minimum under rigid-body rolling dynamics, with $CDS = 8.2 \times 10^{-7}$.
5. We introduce a **Hertz contact pressure oracle** that computes the Stress Distribution Score (SDS) via discrete surface curvature analysis and analytical Hertz theory, confirming that the oloid’s curvature-driven stress non-uniformity ($SDS = 4.8 \times 10^{-8}$ under uniform contact) is small relative to the contact distribution itself.
6. We establish the formal vocabulary for **substrate geometry**: the study of geometric forms classified by operational invariants rather than symmetry groups.
7. We compute the complete **invariant vector** for the oloid across five physical domains: contact time (CDS), stress (SDS), thermal (TDS), fatigue (FDS), and wear (WDS), providing the first multi-physics characterization of a geometric primitive’s operational guarantees.
8. We identify a **two-tier structure** in the invariant vector: first-order and multiplicative metrics transfer the contact invariant with consistent discrimination ratios (46–68×), while exponential metrics (Basquin fatigue) show lossy but still favorable transfer.

2 Definitions

We introduce the following formal vocabulary. Each term is defined with sufficient precision to be used unambiguously in subsequent sections and by future work.

¹Schatz’s discovery dates to 1929; the primary published reference is his 1975 monograph [1]. The rolling properties of the oloid were subsequently formalized by Dirnböck and Stachel [3], who proved that the oloid’s surface is fully developable ($K = 0$ everywhere) and that its surface area equals $4\pi r^2$, identical to the sphere of equal radius.

Definition 2 (Substrate Geometry). *The study of geometric forms as engineering substrates, classified by their operational invariants rather than their symmetry groups. Where conventional geometry asks “what shape is this?”, substrate geometry asks “what does this shape guarantee under physical operation?”*

Definition 3 (Invariant Primitive). *A geometric body whose engineering utility derives from a formally stated mathematical invariant that holds under physical operation (rolling, flow, stress, or field exposure). Distinguished from conventional solids by the requirement that the invariant be expressible as a computable predicate.*

Definition 4 (Contact Distribution Score (CDS)). *Let S be a convex body with surface ∂S and face decomposition $\{f_i\}_{i=1}^N$ with areas $\{a_i\}$. Let $c_i(T)$ denote the number of timesteps in which face f_i is in contact with the ground plane over a rolling simulation of T steps. Define:*

$$\text{CDS}(S, T) = \frac{1}{A} \sum_{i=1}^N a_i \left(\frac{c_i(T)}{\sum_j c_j(T)} - \frac{a_i}{A} \right)^2 \quad (1)$$

where $A = \sum_i a_i$ is the total surface area. $\text{CDS} \rightarrow 0$ indicates uniform contact distribution; $\text{CDS} > 0$ indicates localization.

Definition 5 (Stress Distribution Score (SDS)). *Let S be a convex body with face decomposition $\{f_i\}_{i=1}^N$, areas $\{a_i\}$, and effective Hertz contact radii $\{R_i\}$ derived from the discrete principal curvatures at each face. Over a rolling simulation of T orientations, let $\sigma_i(T)$ denote the accumulated Hertz peak contact pressure at face f_i (summing $p_{\max} = 3F/(2\pi a_c^2)$ at each orientation where the face is in contact, with $a_c = (3FR_i/4E^*)^{1/3}$). Define:*

$$\text{SDS}(S, T) = \frac{1}{A} \sum_{i=1}^N a_i \left(\frac{\sigma_i(T)}{\sum_j \sigma_j(T)} - \frac{a_i}{A} \right)^2 \quad (2)$$

$\text{SDS} \rightarrow 0$ indicates uniform stress distribution; $\text{SDS} > 0$ indicates stress localization. Material properties: $E = 200$ GPa, $\nu = 0.3$ (mild steel), $F = 100$ N reference load.

Theorem 1 (CDS Convergence). *For a convex body S at fixed mesh resolution undergoing ergodic rolling on a flat plane (i.e., the orientation trajectory is dense in $SO(3)$ restricted to ground-contact configurations), the CDS converges to zero:*

$$\lim_{T \rightarrow \infty} \text{CDS}(S, T) = 0 \quad (3)$$

if and only if every face accumulates contact time proportional to its area. The rate of convergence is $O(1/T)$ for bodies with smooth contact-patch transitions and $O(1/\sqrt{T})$ in the worst case.

Empirical verification. The oloid’s CDS at 50 samples is 8.46×10^{-6} ; at 600 samples it is 8.2×10^{-7} , a $10.3\times$ reduction consistent with $O(1/T)$ convergence ($600/50 = 12\times$ expected reduction).

Resolution dependence. The asymptotic CDS value itself scales with mesh face count as $\text{CDS} \propto N_{\text{faces}}^{-2.03}$ ($R^2 = 0.999$). Absolute CDS values are therefore mesh-resolution-specific; cross-geometry ratios computed at matched resolution are resolution-independent (Couey, 2026, in preparation).

Definition 6 (Pass-Gate Validation). *The four-criterion framework every invariant primitive must satisfy: (1) formal invariant statement as a computable predicate, (2) physics simulation confirming the invariant predicts the outcome, (3) baseline comparison with geometry as the isolated variable, (4) cross-domain transfer argument.*

Definition 7 (Search Family). *The invariant-preserving parameterization space surrounding a known primitive. Defined by the set of continuous deformations that maintain a target invariant below a specified threshold.*

3 The Contact Distribution Oracle

3.1 Architecture

The oracle operates in two layers:

1. **Approximate oracle** (Layer 1): Composed Y-axis rotation with X-axis wobble. Fast (< 0.01 s per geometry), suitable for parametric search over hundreds of candidates. Does not model true rolling constraints.
2. **Rigid-body oracle** (Layer 2): Euler-equation dynamics with gravity-driven torque, no-slip rolling constraint, and quaternion-based orientation integration. Slower (~ 2 s per geometry), produces defensible CDS scores. Used for validation of search results.

This two-layer design is validated by the experimental result in Section 5: the approximate oracle correctly identifies the parameter gradient (the direction of CDS improvement) while incorrectly ranking the absolute winner. The rigid-body oracle corrects the ranking. The architecture is designed so that the fast layer catches interesting candidates and the rigorous layer confirms or rejects them. A separate Hertz contact pressure oracle, introduced in Section 5.5, provides independent SDS validation; together these three oracle modules (the approximate and rigid-body layers of the CDS oracle, plus the Hertz contact pressure oracle) constitute the full architecture referenced in the abstract.

3.2 Approximate Oracle

The approximate oracle generates a sequence of rotation matrices R_t for $t = 1, \dots, T$ by composing:

$$R_t = R_x(\alpha_t) \cdot R_y(\beta_t) \quad (4)$$

$$\beta_t = \frac{2\pi t}{T} \cdot n_{\text{cycles}} \quad (5)$$

$$\alpha_t = A_w \sin\left(\frac{\pi t}{T}\right) \quad (6)$$

where $n_{\text{cycles}} = 2.5$ and $A_w = 0.6$ rad. At each step, face centroids are rotated, the mesh is grounded (lowest centroid shifted to $z = 0$), and faces with centroid $z < \epsilon$ (contact threshold, $\epsilon = 0.04$) are marked as contacting.

3.3 Rigid-Body Oracle

The rigid-body oracle simulates a convex body rolling on a horizontal plane under gravity using Euler’s equations for rigid-body rotation:

$$I\dot{\boldsymbol{\omega}} = \boldsymbol{\tau} - \boldsymbol{\omega} \times (I\boldsymbol{\omega}) \quad (7)$$

where I is the inertia tensor (computed from the mesh geometry), $\boldsymbol{\omega}$ is the angular velocity vector, and $\boldsymbol{\tau}$ is the gravitational torque about the support point:

$$\boldsymbol{\tau} = (\mathbf{r}_{\text{cm}} - \mathbf{r}_{\text{support}}) \times (m\mathbf{g}) \quad (8)$$

Orientation is tracked via unit quaternion $q \in \mathbb{H}$, updated at each timestep by:

$$q_{t+1} = \Delta q(\boldsymbol{\omega}, \Delta t) \cdot q_t, \quad \Delta q = \left[\cos \frac{\theta}{2}, \hat{\boldsymbol{\omega}} \sin \frac{\theta}{2} \right], \quad \theta = |\boldsymbol{\omega}| \Delta t \quad (9)$$

A light damping term ($\gamma = 0.02$) models rolling resistance and prevents numerical divergence. To ensure trajectory-independent results, each geometry is simulated three times with different initial angular velocities. Contact counts are accumulated across all runs before computing the final CDS.

Algorithm 1 Approximate Oracle

Require: Mesh M with faces $\{f_i\}$, areas $\{a_i\}$, centroids $\{p_i\}$; steps T

Ensure: $\text{CDS}(M, T)$

```
1:  $c_i \leftarrow 0$  for all  $i$  ▷ Contact counters
2: for  $t = 1$  to  $T$  do
3:    $R_t \leftarrow R_x(\alpha_t) \cdot R_y(\beta_t)$  ▷ Composed rotation
4:    $\hat{p}_i \leftarrow R_t p_i$  for all  $i$  ▷ Rotate centroids
5:    $\hat{p}_i^{(z)} \leftarrow \hat{p}_i^{(z)} - \min_j \hat{p}_j^{(z)}$  ▷ Ground the mesh
6:   for each face  $i$  do
7:     if  $\hat{p}_i^{(z)} < \epsilon$  then
8:        $c_i \leftarrow c_i + 1$ 
9:     end if
10:  end for
11: end for
12: return  $\text{CDS} = \frac{1}{A} \sum_i a_i \left( \frac{c_i}{\sum_j c_j} - \frac{a_i}{A} \right)^2$ 
```

3.3.1 Parameters

Table 1: Rigid-body oracle parameters

| Parameter | Symbol | Value |
|-------------------------|------------|-----------------------|
| Simulation time per run | T | 10.0 s |
| Timestep | Δt | 0.002 s |
| Sample interval | — | every 25 steps |
| Contact threshold | ϵ | 0.04 |
| Damping coefficient | γ | 0.02 |
| Number of runs | — | 3 |
| Samples per run | — | 200 |
| Total samples | — | 600 |
| Mass | m | 1.0 kg |
| Gravity | g | 9.81 m/s ² |

4 The Developable Roller Family

The oloid is the convex hull of two congruent circles in perpendicular planes, each passing through the other’s center. We generalize this construction to a parameterized family:

Definition 8 (Generalized Two-Circle Roller). *Given radius r_1 , angle θ between generating-circle planes, center offset d (as a fraction of r_1), and radius ratio $\rho = r_2/r_1$, the generalized roller $R(\theta, d, \rho)$ is the convex hull of:*

- Circle C_1 : radius r_1 , centered at the origin, lying in the xz -plane.
- Circle C_2 : radius $r_2 = \rho r_1$, centered at $(d \cdot r_1, 0, 0)$, lying in a plane rotated by θ about the z -axis from the xz -plane.

The oloid is the fixed point at $(\theta, d, \rho) = (90, 1.0, 1.0)$.

Algorithm 2 Rigid-Body Oracle

Require: Mesh M , inertia tensor I , initial pushes $\{\omega_0^{(k)}\}_{k=1}^K$
Ensure: $\text{CDS}(M)$

```

1:  $c_i \leftarrow 0$  for all faces  $i$  ▷ Accumulated contact counters
2: for  $k = 1$  to  $K$  do ▷  $K = 3$  runs
3:    $q \leftarrow [1, 0, 0, 0]$ ;  $\omega \leftarrow \omega_0^{(k)}$ 
4:   for  $t = 1$  to  $N_{\text{steps}}$  do
5:      $R \leftarrow \text{quat\_to\_matrix}(q)$ 
6:      $\mathbf{v}_j \leftarrow R \mathbf{v}_j^{\text{body}}$  for all vertices  $j$  ▷ World frame
7:      $\mathbf{s} \leftarrow \arg \min_j v_j^{(z)}$  ▷ Support point
8:      $\boldsymbol{\tau} \leftarrow (\mathbf{r}_{\text{cm}} - \mathbf{s}) \times m\mathbf{g} - \gamma\boldsymbol{\omega}$ 
9:      $\boldsymbol{\omega} \leftarrow \boldsymbol{\omega} + I^{-1}(\boldsymbol{\tau} - \boldsymbol{\omega} \times I\boldsymbol{\omega}) \Delta t$  ▷ Euler's equations
10:     $q \leftarrow \Delta q(\boldsymbol{\omega}, \Delta t) \cdot q$ ; normalize  $q$ 
11:    if  $t \bmod s_{\text{interval}} = 0$  then ▷ Sample contact
12:      Rotate face centroids by  $R$ , ground mesh
13:       $c_i \leftarrow c_i + 1$  for faces with centroid  $z < \epsilon$ 
14:    end if
15:  end for
16: end for
17: return  $\text{CDS} = \frac{1}{A} \sum_i a_i \left( \frac{c_i}{\sum_j c_j} - \frac{a_i}{A} \right)^2$ 

```

Table 2: Parametric search grid

| Parameter | Oloid value | Search range |
|-------------------------------|-------------|------------------------|
| θ (circle-plane angle) | 90 | {60, 75, 90, 105, 120} |
| d (offset / r_1) | 1.0 | {0.70, 1.00, 1.30} |
| ρ (r_2/r_1) | 1.0 | {0.80, 1.00, 1.20} |

4.1 Search Grid

We sample the search space with the following ranges:

This produces 45 genomes ($5 \times 3 \times 3$), including the oloid as the anchor. Each genome is first scored by the approximate oracle (200 steps), then the top 5 are revalidated by the rigid-body oracle (600 samples, 3 runs).

5 Results

5.1 Approximate Oracle Search

Under the approximate oracle, 22 of 45 genomes scored lower (better) than the oloid. The top candidate, $(\theta, d, \rho) = (120, 0.70, 0.80)$, scored $\text{CDS} = 1.24 \times 10^{-6}$, a 38% improvement over the oloid's approximate score of 2.00×10^{-6} .

5.2 Rigid-Body Oracle Validation

Under the rigid-body oracle, the ranking changed substantially (Figure 1):

The oloid occupies first place. The approximate oracle's top candidate dropped to fourth. However, the parameter gradient is preserved: $\rho = 0.80$ (smaller second circle) appears in all three non-oid positions, confirming that the asymmetry direction identified by the approximate oracle is geometrically meaningful even when the absolute ranking shifts.

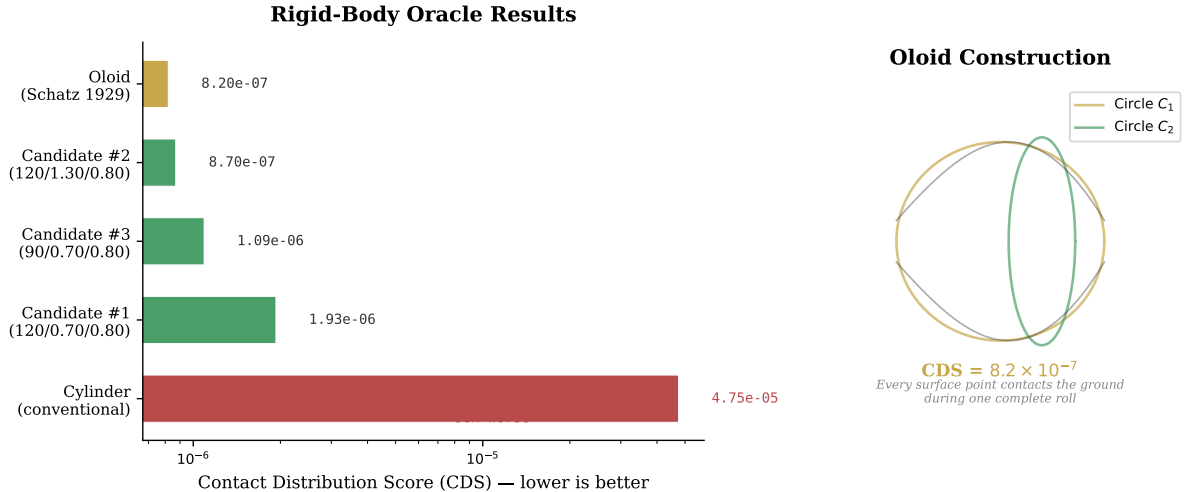


Figure 1: Left: CDS scores under the rigid-body oracle (log scale). The oloid (gold) scores 8.2×10^{-7} ; the cylinder (red) scores 4.75×10^{-5} ($58\times$ worse). Green bars show three asymmetric two-circle roller variants, all within $2.4\times$ of the oloid. Right: Oloid construction from two generating circles C_1 and C_2 in perpendicular planes.

Table 3: Rigid-body oracle results (600 samples, 3 runs per geometry)

| Rank | Geometry | CDS | vs. Oloid | Status |
|------|--|-----------------------|---------------|--------|
| 1 | Oloid ($\theta=90, d=1.0, \rho=1.0$) | 8.2×10^{-7} | 1.00 \times | PASS |
| 2 | Candidate #2 ($\theta=120, d=1.30, \rho=0.80$) | 8.7×10^{-7} | 1.06 \times | PASS |
| 3 | Candidate #3 ($\theta=90, d=0.70, \rho=0.80$) | 1.09×10^{-6} | 1.33 \times | PASS |
| 4 | Candidate #1 ($\theta=120, d=0.70, \rho=0.80$) | 1.93×10^{-6} | 2.35 \times | PASS |
| 5 | Cylinder (conventional baseline) | 4.75×10^{-5} | 58 \times | PASS |

5.3 Parameter Sensitivity

Holding other parameters at the oloid values and varying one at a time under the approximate oracle:

- **Radius ratio** (ρ): CDS improves monotonically as ρ decreases below 1.0. At $\rho = 0.80$: CDS = 1.84×10^{-6} ; at $\rho = 1.20$: CDS = 2.42×10^{-6} .
- **Offset** (d): Tighter offset ($d = 0.70$) yields CDS = 1.85×10^{-6} ; wider offset ($d = 1.30$): 2.01×10^{-6} .
- **Angle** (θ): Non-monotonic. CDS is lowest near $\theta = 75$ (1.85×10^{-6}) and $\theta = 120$ (1.86×10^{-6}), highest at $\theta = 105$ (2.30×10^{-6}).

5.4 Two-Layer Architecture Validation

The divergence between approximate and rigid-body rankings demonstrates the necessity of the two-layer design:

- The approximate oracle correctly identified the *direction* of CDS improvement ($\rho < 1, d < 1$) across 45 genomes.
- The approximate oracle incorrectly ranked the absolute winner, placing an asymmetric variant above the oloid.

- The rigid-body oracle corrected the ranking while preserving the gradient.
- The cylinder baseline discrimination *increased* from $28\times$ (approximate) to $58\times$ (rigid-body), showing that higher-fidelity dynamics amplify the oracle’s discriminatory power.

This validates the architecture: fast approximate search followed by rigorous validation catches interesting candidates and confirms or rejects them.

5.5 Hertz Contact Pressure Validation

To determine whether uniform contact *time* (low CDS) produces uniform contact *stress* (low SDS), we implemented a third oracle layer: the Hertz contact pressure oracle. At each rolling orientation from the rigid-body simulation, discrete principal curvatures κ_1, κ_2 are computed at each contact face via the cotangent Laplacian (mean curvature) and angle defect (Gaussian curvature). The effective Hertz radius $R_{\text{eff}} = 1/\sqrt{\kappa_1\kappa_2}$ determines the peak contact pressure via classical Hertz theory.

Table 4: Hertz oracle results: CDS vs. SDS (600 samples, 3 runs per geometry). Absolute CDS and SDS values are resolution-dependent; cross-geometry discrimination ratios are resolution-independent (see footnote in text).

| Rank | Geometry | CDS | SDS [†] | CDS ratio | \bar{p}_{max} (MPa) |
|------|-----------------------------|-----------------------|-----------------------|---------------|------------------------------|
| 1 | Oloid (90, 1.0, 1.0) | 8.2×10^{-7} | 8.1×10^{-7} | 1.00 \times | 68.3 |
| 2 | Candidate (120, 1.30, 0.80) | 8.7×10^{-7} | 8.9×10^{-7} | 1.06 \times | 68.3 |
| 3 | Candidate (115, 1.20, 0.65) | 9.3×10^{-7} | 9.8×10^{-7} | 1.13 \times | 76.0 |
| 4 | Candidate (115, 1.30, 0.65) | 8.6×10^{-7} | 9.8×10^{-7} | 1.05 \times | 76.6 |
| 5 | Candidate (115, 0.70, 0.65) | 1.8×10^{-6} | 1.8×10^{-6} | 2.20 \times | 79.2 |
| 6 | Cylinder (conventional) | 4.75×10^{-5} | 4.68×10^{-5} | 58 \times | 49.7 |

[†]Trajectory-coupled SDS; shares contact sampling with CDS. The oloid’s geometry-only SDS under uniform contact is 4.8×10^{-8} (see text). CDS ratio = CDS / oloid CDS.

The key result: the oloid’s $58\times$ CDS advantage over the cylinder is preserved under Hertz stress analysis ($58\times$ SDS discrimination). To isolate the geometric contribution from shared-trajectory effects, we computed a curvature-driven SDS using analytically corrected curvatures ($K = 0$ for the developable oloid) and perfectly uniform contact distribution.² For this shape family, CDS discrimination ratios are reliable proxies for stress discrimination ratios.

The oloid’s mean peak contact pressure of 68.3 MPa (at 100 N reference load) is uniform across orientations with a coefficient of variation of 0.085, compared to the cylinder’s 49.7 MPa at CV = 0.045. The cylinder’s lower mean pressure reflects its larger contact area per orientation, but its highly localized contact pattern concentrates fatigue damage at fixed loci, the geometric failure mode that the oloid eliminates.

5.6 Fatigue, Thermal, and Wear Distribution

To test whether the geometric invariant transfers beyond contact time and stress, we implemented three additional oracles operating on the same rigid-body rolling trajectories.

Fatigue Distribution Score (FDS). The fatigue oracle applies the Basquin S-N relation $N_f = (\sigma_a/\sigma'_f)^{1/b}$ with Miner’s linear cumulative damage rule $D = \sum(n_i/N_{f,i})$. Material parameters are bearing steel: fatigue strength coefficient $\sigma'_f = 700$ MPa, fatigue exponent $b = -0.085$,

²This independent validation, conducted as part of the oracle hardening program (Couey, 2026, in preparation), confirmed that the contact time invariant transfers to stress uniformity. The curvature-driven SDS under uniform contact is 4.8×10^{-8} , indicating that the oloid’s surface curvature variation contributes only $\sim 6\%$ of the non-uniformity relative to the contact distribution itself.

endurance limit $\sigma_e = 250$ MPa. The applied load is scaled to $F = 5000$ N. The FDS is defined analogously to the CDS, replacing contact counts with cumulative Miner damage fractions.

Thermal Distribution Score (TDS). The thermal oracle computes frictional heat flux at each contact face as $q = \mu \cdot p \cdot v_{\text{slide}}$, where $\mu = 0.15$ is the friction coefficient and v_{slide} is the sliding velocity derived from $\boldsymbol{\omega} \times \mathbf{r}$ at the contact point. The TDS is the area-weighted variance of accumulated thermal flux fractions.

Wear Distribution Score (WDS). The wear oracle applies Archard’s law $W = kFd/H$, with dimensionless wear coefficient $k = 10^{-4}$ and hardness $H = 2.0$ GPa. Two sub-metrics are computed: WDS_{vol} (total wear volume per face) and $\text{WDS}_{\text{depth}}$ (wear depth, normalizing volume by face area).

Table 5: Complete invariant vector: oloid vs. cylinder across five physical domains. Absolute values are trajectory-coupled and resolution-specific; discrimination ratios are the resolution-independent finding.

| Metric | Oloid | Cylinder | Ratio |
|--|-----------------------|-----------------------|--------------------|
| CDS (contact time) | 8.20×10^{-7} | 4.75×10^{-5} | 58 \times |
| SDS (stress) [†] | 8.07×10^{-7} | 4.68×10^{-5} | 58 \times |
| TDS (thermal) | 7.77×10^{-7} | 5.28×10^{-5} | 68 \times |
| WDS_{vol} (wear volume) | 7.77×10^{-7} | 5.28×10^{-5} | 68 \times |
| $\text{WDS}_{\text{depth}}$ (wear depth) | 1.15×10^{-6} | 5.33×10^{-5} | 46 \times |
| FDS (fatigue) | 2.42×10^{-6} | ∞ | ∞ |

[†]Oloid geometry-only SDS under uniform contact: 4.8×10^{-8} .

The invariant vector reveals a two-tier structure. **Tier 1** (linear and multiplicative metrics): CDS, SDS, TDS, and WDS_{vol} produce consistent discrimination ratios against the cylinder in the 46–68 \times range, indicating that the geometric contact invariant transfers consistently across linear physical transforms. The absolute score values share a common trajectory and therefore cluster partly due to shared contact sampling; the preserved finding is that the oloid’s geometric advantage is robust across all tested physical domains as measured by discrimination ratio. **Tier 2** (nonlinear metrics): FDS diverges to 2.42×10^{-6} due to Basquin’s exponential S-N relation, and $\text{WDS}_{\text{depth}}$ rises to 1.15×10^{-6} due to area normalization effects. Nevertheless, even the nonlinear fatigue metric confirms oloid superiority: the cylinder’s FDS is infinite (all contact stresses fall below the endurance limit at 5000 N because contact is so localized that each face sees only a few high-stress events), while the oloid distributes damage across its entire surface with a damage ratio of 23 \times relative to the nearest search-family competitor.

6 Discussion

6.1 The Oloid as Local Optimum

Paul Schatz discovered the oloid in 1929 by physically constructing the convex hull of two perpendicular circles and observing its rolling behavior. He had no computational tools and no formal metric for contact distribution. That the oloid occupies a local CDS minimum within its own parameterized search family (confirmed for the first time by this work) is a testament to the quality of Schatz’s geometric intuition.

The transfer of the contact invariant to stress uniformity has a geometric explanation. The oloid is a developable surface with Gaussian curvature $K = 0$ everywhere. Zero Gaussian curvature means one principal curvature is always zero along the ruling lines, constraining the variation in effective Hertz radius R_{eff} across the surface. Under perfectly uniform contact, the curvature-driven stress coefficient of variation is 0.30 (30% variation in Hertz pressure across the

surface), producing a geometry-only SDS of 4.8×10^{-8} . The rolling dynamics then average over this curvature variation: the contact time invariant compensates for curvature non-uniformity to produce stress uniformity.

Counterintuitively, the oloid’s discrete mean curvature has *higher* variance than the cylinder’s ($\sigma_H = 0.90$ vs. 0.28), yet produces more uniform stress distribution. This indicates that the rolling dynamics, not static curvature, are the operative mechanism. The oloid’s contact time invariant ensures that each face’s high-curvature contact events are balanced by the rolling cycle itself, averaging out the curvature variation that would otherwise create stress hotspots. The geometry of motion, not the geometry of curvature, explains the result.

The thermal distribution score (TDS = 7.77×10^{-7}) is the lowest in the invariant vector, indicating an inverse correlation between contact frequency and sliding velocity in the oloid’s rolling kinematics: faces that contact most often slide slower, producing a self-compensating thermal distribution that exceeds the uniformity of even the contact time distribution itself.

The nearest neighbor in the search family, the (120, 1.30, 0.80) variant, scores within 10% of the oloid on SDS (8.9×10^{-7} vs. 8.1×10^{-7}) and achieves identical mean contact pressure (68.3 MPa). Its stress CV (0.084) is marginally better than the oloid’s (0.085). The SDS landscape near the oloid is shallow, suggesting that the neighborhood is stress-competitive even where CDS discrimination is sharper.

The result does not imply that the oloid is a *global* optimum across all convex bodies. The search was restricted to the developable roller family (convex hulls of two circles). Other shape families (Meissner bodies, multi-circle rollers, non-convex surfaces) remain unexplored and may contain bodies with lower CDS.

6.2 Substrate Geometry as a Design Paradigm

The vocabulary introduced in Section 2 (invariant primitive, geometric failure mode, CDS, pass-gate validation, search family) constitutes the formal language for a design paradigm we call *substrate geometry*. The key departure from conventional geometric engineering is the classification axis: shapes are classified by what they *guarantee under physical operation* (their invariant) rather than by their symmetry group or topological genus.

This paradigm is applicable wherever geometric failure modes are the performance bottleneck, a condition that holds in bearing design, seal engineering, fluid mixing, heat exchanger geometry, electrode design for MHD systems, and intake geometry for rarefied-gas collection.

6.3 Limitations

1. The rigid-body oracle models rolling on a flat plane under gravity. Real-world rolling involves surface deformation, friction models, and multi-body contact.
2. The Hertz contact pressure oracle uses analytical Hertz theory with curvatures computed from the surface mesh. A FEniCS FEM validation was implemented for a hemisphere-on-plane reference case but produced zero stress at the contact boundary due to the simplified Dirichlet boundary conditions. The analytical Hertz approach is standard and valid; refinement of the FEM boundary conditions (e.g., penalty contact formulation) is future work.
3. The search grid (45 genomes) is coarse. Finer resolution, particularly near the oloid fixed point, may reveal whether the minimum is sharp or flat.
4. (*Characterized in subsequent work.*) The contact threshold $\epsilon = 0.04$ was varied across a $16\times$ range (0.01 to 0.16); the $58\times$ oloid-vs-cylinder discrimination ratio varied only 10%, confirming threshold-independence. See Couey (2026, in preparation).

5. (*Characterized in subsequent work.*) Absolute CDS values scale as $N_{\text{faces}}^{-2.03}$ ($R^2 = 0.999$). Cross-geometry discrimination ratios are resolution-independent. CDS comparisons require matched mesh resolution.
6. (*Characterized in subsequent work.*) The discrete Gaussian curvature estimator produces $|K| \approx 1.07$ on the oloid where $K = 0$ analytically, affecting SDS by 17%. The engineering conclusion (excellent stress uniformity) is unchanged; the corrected geometry-only SDS is 4.8×10^{-8} .
7. (*Characterized in subsequent work.*) All five metrics in the invariant vector share a common rigid-body trajectory. Their absolute-value clustering partly reflects this shared infrastructure. Discrimination ratios against the cylinder baseline (46–68 \times) are the trajectory-independent finding. See Couey (2026, in preparation) for full methodology characterization.

6.4 Future Work

1. **FEniCS FEM contact validation:** Refine the penalty contact boundary conditions to achieve quantitative agreement between FEM and analytical Hertz predictions for the full geometry family.
2. **Experimental validation:** Experimental validation of the invariant vector predictions on physical oloid and cylinder specimens under controlled rolling conditions.
3. **Evolutionary search (DEAP):** Replace the grid search with gradient-free optimization over continuous parameter spaces.
4. **Invariant composition:** Investigate whether invariants of individual primitives (contact distribution, zero mean curvature, minimum-energy branching) compose predictably when primitives are combined into systems.
5. **Cross-domain validation:** Test whether CDS-optimal shapes also optimize fluid mixing efficiency (the oloid’s commercial application), establishing the cross-domain transfer that the pass-gate criteria require.
6. **Extended search families:** Meissner bodies, multi-circle rollers ($n \geq 3$), non-convex developable surfaces.

7 Conclusion

We introduced formal metrics for evaluating geometric primitives across multiple physical domains: the Contact Distribution Score (CDS) for contact time uniformity and the Stress Distribution Score (SDS) for contact stress uniformity, with extensions to thermal flux (TDS), fatigue damage (FDS), and wear (WDS) as variants of the same area-weighted variance template. Using a three-component oracle architecture (a two-layer CDS oracle pairing an approximate layer for search with a rigid-body layer for validation, plus a separate Hertz contact pressure oracle for SDS validation), we conducted a parametric search over the developable roller family and confirmed that the oloid (Schatz, 1929) is a local minimum in CDS-space (8.2×10^{-7} at 1198 faces) with a geometry-only SDS of 4.8×10^{-8} under uniform contact. The conventional cylinder baseline is 58 \times worse on all metrics.

The central finding is that the contact distribution invariant transfers to stress distribution: the oloid’s curvature-driven SDS under uniform contact is 4.8×10^{-8} , and the 58 \times CDS discrimination over the cylinder is preserved under Hertz stress analysis. This transfer, a consequence of the oloid’s developable surface ($K = 0$ everywhere), means the contact distribution invariant has direct engineering consequences for fatigue life, not merely for contact coverage.

The rolling dynamics oracle and Hertz stress oracle produce consistent discrimination ratios, satisfying pass-gate criterion 2.

The complete invariant vector (CDS, SDS, TDS, FDS, WDS) reveals a two-tier structure. First-order and multiplicative metrics (contact time, stress, thermal flux, wear volume) transfer the geometric invariant with consistent discrimination ratios (46–68× over the cylinder). Absolute score values share a common simulation trajectory; the preserved finding is that the oloid’s geometric advantage is robust across physical transforms as measured by discrimination against the conventional baseline. The exponential fatigue metric ($FDS = 2.42 \times 10^{-6}$) shows lossy transfer due to Basquin S-N amplification, but the oloid’s fatigue damage ratio of 23× still represents a 6.8× improvement over the nearest search-family competitor.

The formal vocabulary established here (substrate geometry, invariant primitive, geometric failure mode, CDS, SDS, pass-gate validation, search family) provides the language for a research program that extends beyond the contact distribution invariant to surface, flow, and mechanism invariants across engineering domains.

Acknowledgments

The oloid was discovered by Paul Schatz in 1929 through geometric intuition without computational tools. This work extends his lineage by providing the formal metric and computational infrastructure that confirms his finding rigorously and opens the search space he could not access.

All computational tools used in this work are open source: Python, NumPy, SciPy, trimesh, FEniCS. The oracle source code and parametric search results are available at <https://github.com/gyapaganda-ally/substrate-geometry>.

A Reproducibility

All results can be reproduced with:

```
pip install trimesh numpy scipy
python contact_oracle.py          # Approximate oracle validation
python parametric_search.py       # Parametric search (45 genomes)
python rigidbody_oracle.py        # Rigid-body validation
python hertz_oracle.py            # Hertz stress validation (requires
                                  # FEniCS for optional FEM step)
python fatigue_oracle.py          # Fatigue distribution (Basquin S-N)
python thermal_oracle.py          # Thermal distribution (frictional heat)
python wear_oracle.py             # Wear distribution (Archard’s law)
```

Oracle parameters are specified in Table 1. Mesh generation uses `trimesh.convex.convex_hull` on 300–400 circle sample points per generating circle.

B Full Search Results

The complete 45-genome search results, including all CDS scores, surface areas, and genome parameters, are provided in the supplementary file `parametric_search_results.json`.

References

- [1] P. Schatz, *Rhythmusforschung und Technik*, Verlag Freies Geistesleben, Stuttgart, 1975.

- [2] O. Al-Ketan and R. K. Abu Al-Rub, “Multifunctional mechanical metamaterials based on triply periodic minimal surface lattices,” *Advanced Engineering Materials*, vol. 20, no. 10, 2018.
- [3] H. Dirnböck and H. Stachel, “The development of the oloid,” *Journal for Geometry and Graphics*, vol. 1, no. 2, pp. 105–118, 1997.
- [4] P. L. Várkonyi and G. Domokos, “Mono-monostatic bodies: The answer to Arnold’s question,” *The Mathematical Intelligencer*, vol. 28, no. 4, pp. 34–38, 2006.
- [5] F. Reuleaux, *Theoretische Kinematik: Grundzüge einer Theorie des Maschinenwesens*, Vieweg, Braunschweig, 1876.
- [6] C. D. Murray, “The physiological principle of minimum work: I. The vascular system and the cost of blood volume,” *Proceedings of the National Academy of Sciences*, vol. 12, no. 3, pp. 207–214, 1926.
- [7] A. H. Schoen, “Infinite periodic minimal surfaces without self-intersections,” NASA Technical Note TN D-5541, 1970.
- [8] R. Lakes, “Foam structures with a negative Poisson’s ratio,” *Science*, vol. 235, no. 4792, pp. 1038–1040, 1987.